

The potential of high-density observations for numerical weather prediction: A study with simulated observations

By Z.-Q. LIU^{1,2*} and F. RABIER¹

¹*Centre National de Recherches Météorologiques, Météo-France, Toulouse, France*

²*National Satellite Meteorological Center, Beijing, China*

(Received 12 August 2002; revised 21 February 2003)

SUMMARY

The skill of numerical weather prediction depends to a large extent upon the quantity of globally available observations. Only a fraction of the available observations (especially high-density observations) is used in current operational assimilation systems. In this paper, the potential of high-density observations is studied in a practical four-dimensional variational assimilation context. Two individual meteorological situations are used to examine the impact of different observation densities on the analysis and the forecast. A series of observing-system simulation experiments are performed. Both direct observations (temperature and surface pressure) and indirect observations (radiance) are simulated, with uncorrelated or correlated errors. In general, it is verified that a small reduction (increase) of the initial error in a sensitive area can produce a considerable improvement (degradation) of the targeted forecast. In particular, the results show that increasing the observation density for the uncorrelated-error case can generally improve the analysis and the forecast. However, for correlated observation errors and the use of a diagonal observation-error covariance matrix in the assimilation, an increase in the observation number such that the error correlation between two adjacent observations becomes greater than a threshold value (around 0.2) degrades the analysis and the forecast. Posterior diagnostics of the sub-optimality of the assimilation scheme for correlated observation errors are analysed. Finally, it is shown that a risk of using high-density observations and poor vertical resolution is that deficiencies in the background-error statistics can lead to unrealistic analysis increments at some levels where no observations are present, and so produce a degradation of the analysis at these levels.

KEYWORDS: NWP sensitivity Observation-error correlation Observation thinning OSSEs

1. INTRODUCTION

The performance of current numerical weather-prediction (NWP) systems benefits to a large extent from the increasing amount of globally available remotely-sensed observations used together with conventional observations to generate initial conditions for forecasts. Some of these data, such as raw radiances from the Advanced TIROS† Operational Vertical Sounder (ATOVS) on board NOAA‡ satellites, have fine horizontal resolutions. The observation spacing can be smaller than the analysis grid of global NWP models. Not all of these observations are used in data assimilation systems because of the following three considerations. Firstly, current computing and storage power limits the use of all observations. This will be even more true for next generation sensors, such as AIRS (Atmospheric InfraRed Sounder) and IASI (Infrared Atmospheric Sounding Interferometer), that will provide thousands of radiances in each pixel. It will be necessary to reduce the quantity of data used in the system, for instance by selecting the most useful channels (Rabier *et al.* 2002). Secondly, the vertical resolution of current ATOVS sensors is generally thought not to be enough to allow the use of these data at high horizontal densities. Indeed, Lindzen and Fox-Rabinovitz (1989) and Fox-Rabinovitz and Lindzen (1993) suggested that observations with a fine horizontal resolution accompanied by a sparse vertical resolution might produce increased analysis noise. The third reason (and probably the most important one) is that the errors affecting

* Corresponding author: National Satellite Meteorological Center, 46 South Zhong Guan Cun Street, Beijing 100081, China. e-mail: zqliu@nsmc.cma.gov.cn

† Television InfraRed Operational Satellite.

‡ National Oceanic and Atmospheric Administration.

© Royal Meteorological Society, 2003.

these remotely-sensed observations may be horizontally correlated; current assimilation systems do not generally consider this correlation in the modelling of the observation-error covariance, because of both a lack of accurate information on the correlation statistics and the technical difficulty of implementation. Alternatively, most NWP centres tend to use sub-optimal schemes for which the observation-error covariance matrix is designed to be diagonal. At the same time, horizontal thinning of remotely-sensed observations is performed in order to reduce their effective error correlation (Järvinen and Undén 1997).

Liu and Rabier (2002) (denoted by LR2002 hereafter) have shown, in a simple one-dimensional context, that using more observations with uncorrelated errors can always improve the analysis accuracy. For observations with correlated errors and the use of a diagonal observation-error covariance matrix, a correlation coefficient of about 0.15 between two adjacent observations seems to correspond to a thinning which gives optimal results. The present study attempts to verify further the above conclusion in a practical four-dimensional variational data assimilation system (4DVAR) with simulated observations whose error character is perfectly known. To focus on forecast-performance issues that are critical, the study concentrates on two difficult meteorological situations for which the operational initial fields failed to produce correct forecasts. The problem of consistency of vertical and horizontal resolution is also examined. The paper is organized as follows: in the next section the assimilation and forecast systems used in the study are briefly described; section 3 is devoted to the examination of the effects of observation-error correlation on the analysis and forecast performance; section 4 focuses on the problem of consistency of vertical and horizontal resolution; the conclusion is given in the last section.

2. THE ASSIMILATION AND FORECAST SYSTEM USED FOR THE OSSES

The assimilation and forecast system with which the observing-system simulation experiments (OSSEs) are performed is the French ARPEGE* model, a global spectral model. A specific feature of the model is the use of a stretched grid in the horizontal direction to obtain increased resolution over a geographical area of interest (Courtier and Geleyn 1988). The resolution used in the study is taken to be the same as the operational configuration in use in 2001. In the horizontal, it uses a triangular truncation T199. A terrain-following pressure-based hybrid vertical coordinate η with 31 levels is used, with the top of the model at about 5 hPa. A stretching coefficient 3.5 gives a spectral resolution varying from T696 (199×3.5) over France to T57 ($199 \div 3.5$) over New Zealand. The assimilation component of the system includes a multi-incremental 4DVAR assimilation (Courtier *et al.* 1994; Veersé and Thépaut 1998) with a six-hour assimilation window for the upper-air and surface-pressure fields and an optimal interpolation (OI) analysis for other surface fields. The stretched grid leads to some difficulties as to the specification of the background-error covariances, and so the incremental analysis is performed on a regular unstretched grid in the current implementation. The minimization of the incremental cost function is performed with a successively increased resolutions, namely T42, T63 and T95. In the first two steps of the minimization only the tangent-linear and adjoint of the adiabatic version of the forward forecast model are used (with a simple diffusion scheme). In the third minimization, the tangent-linear and adjoint of a simplified and regular physical parametrization package are introduced (Janisková *et al.* 1999). In addition, an incremental digital-filter initialization (Lynch *et al.* 1997; Gauthier and Thépaut 2001) is used to remove spurious gravity waves.

* Action de Recherche Petite Echelle et Grande Echelle.

Our goal is to understand better the possible optimal configurations between the model resolution and the observation density. It is more convenient to associate the spectral resolution with some more direct indication of resolution, such as the smallest resolvable wavelength. A feature of triangular truncation is that it has globally uniform resolution on the transformed sphere. The smallest resolvable wavelength in a model truncated at total wave number N will be $2\pi a/N$ (a is the radius of the earth). On the real geographical sphere, for a given stretching coefficient C , the smallest resolvable wavelengths are, respectively, $2\pi a/(N \times C)$ over France and $2\pi aC/N$ over New Zealand. This corresponds to a highest resolution of 57 km and the lowest resolution of 704 km for the forecast and the computation of the innovation vector. For the incremental analysis at T95 we have a uniform resolution of 421 km.

3. STUDY OF EFFECT OF OBSERVATION-ERROR CORRELATION STRENGTH

(a) *Meteorological situation and model simulation*

Two severe storms (the so-called French storms) hit Europe on 26–28 December 1999 and caused serious damage. Model forecasts from different operational centres for both storms were generally poor even at a range of 24 hours. However, forecasts from Météo-France verified better than most others. The second storm reached its maximum at 18 UTC 27 December. At that time, a 3DVAR assimilation system was operational at Météo-France. The operational forecast at a range of 54 h (Fig. 1(c)) seriously underestimated the intensity of the storm and misplaced the centre of the depression too far in the south-west direction. This meteorological situation is also an interesting case for which the 4DVAR assimilation significantly improves the analysis and the subsequent forecast. Figure 1(a) shows the verifying pre-operational 4DVAR analysis at 18 UTC 27 December. Figures 1(b) and (c) are the 54-hour forecasts starting from a pre-operational 4DVAR analysis and from an operational 3DVAR analysis, respectively, valid at 12 UTC 25 December. One can see that the central pressure of the forecast is reduced from 976 hPa for the 3DVAR one to 968 hPa for the 4DVAR one, although there is still a 6 hPa difference with respect to the central pressure of 962 hPa in the verifying analysis and a spurious depression appears at (57°N, 15°E). The position of the depression centre is much better predicted by the forecast from the 4DVAR analysis.

(b) *Truth, background and simulated observations*

The OSSEs were based on this second ‘French’ storm. All the OSSEs were performed on the six-hour time window centred at 18 UTC 25 December 1999. We chose the six-hour forecast performed from the 4DVAR analysis at 12 UTC 25 December as the initial ‘truth’, so that the ‘truth’ at the storm time corresponds to the result in Fig. 1(b). Such a definition of the truth implies a perfect-model hypothesis, as is usual in OSSEs of the identical-twin type (Charles *et al.* 1986). The verification of the results of the OSSEs was done by referring to the truth defined above. The background field was a six-hour forecast done from the operational 3DVAR analysis valid at 12 UTC 25 December. The 48-hour forecast from it corresponds to the result in Fig. 1(c). The background error covariance is multivariate and vertically non-separable, as described by Rabier *et al.* (1998) and Derber and Bouttier (1999).

Observations were simulated only in an area critical for the forecast performance. The rationale for this approach is that the skill of the forecast of the storm is determined to a large extent by the analysis in a so-called ‘sensitive area’. The adjoint tools built into the ARPEGE model allowed us to determine the sensitive areas easily. The general procedure for determining a sensitive area using the adjoint method is as follows:

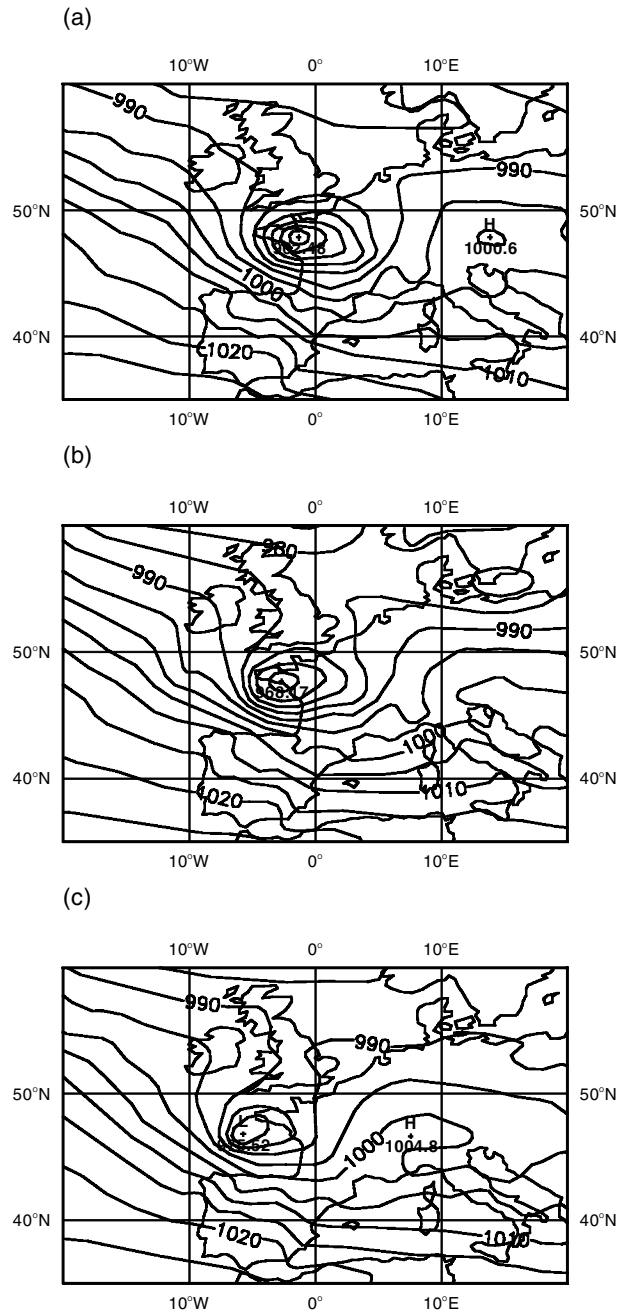


Figure 1. Mean-sea-level pressure fields (contour interval 5 hPa) at 18 UTC 27 December 1999 from (a) the 4DVAR analysis, (b) the 54-hour forecast starting from the 4DVAR analysis at 12 UTC 25 December 1999, and (c) the 54-hour forecast starting from the operational 3DVAR analysis at 12 UTC 25 December 1999. The central pressures are, respectively, 962.48 hPa, 968.17 hPa and 975.52 hPa.

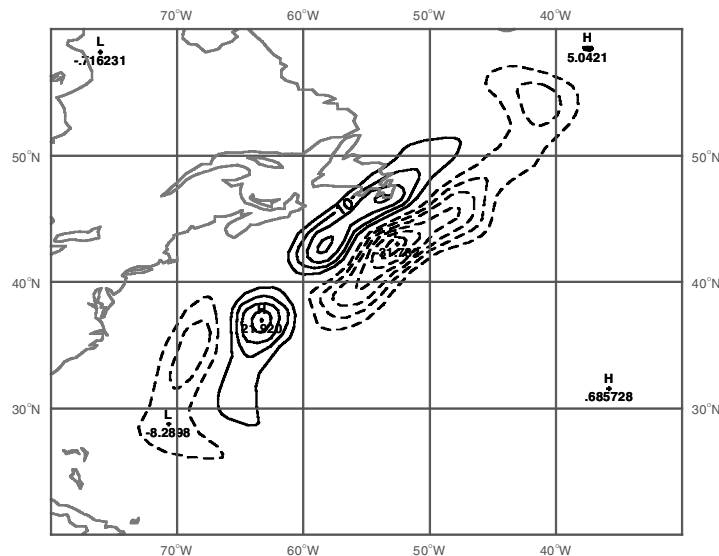


Figure 2. Gradient field of the cost function with respect to 700 hPa temperature at 18 UTC 25 December. The contour interval is 5 K. The gradient value shown has been divided by 10.

(1) choose an area of interest at the target time where the forecast is to be improved; (2) choose a cost function which measures the amplitude of the forecast errors at the target time; (3) perform a forward-model integration to obtain the model trajectory from the initial time to the target time which will be used in the subsequent adjoint integration; and (4) perform a ‘backward’ adjoint-model integration, taking the gradient of the cost function with respect to the forecast at the target time as the initial condition. The result of this adjoint integration is the gradient field of the cost function at the initial time; this is the so-called sensitivity field. A targeted area in a box (43°N – 53°N , 12.5°W – 2.5°E) was chosen for this study. In our simulated framework the reference truth was known perfectly; this allowed us to compute the forecast error precisely using the total-energy-norm type of cost function defined by Rabier *et al.* (1996). Figure 2 shows the gradient field for the temperature at 700 hPa. The area covered by the strong gradient tilts gradually toward the north-west from low to high levels (not shown), a feature also found in the study by Rabier *et al.* (1996). The maximum sensitivity is found in the lower troposphere. We chose the area (30°N – 55°N , 70°W – 40°W), which includes the large sensitivity values, to simulate the observations.

Only the temperature and surface-pressure observations corresponding to the mass field over this area were simulated and assimilated into the system. The simulated temperature and surface-pressure observations were obtained by adding noise to the true field. All observations were supposed to be measured at 18 UTC 25 December (at the analysis time, the centre of the six-hour time window). In addition, in order to avoid the introduction of interpolation errors in the simulation procedure, all data were located at the Gaussian grid points of the forecast model on all 31 model levels. This way of simulating the observations implies that the observations have the same resolution as the forecast model at the corresponding grid points, so that they can be considered as some sort of remotely-sensed measurements rather than as in-situ (point) measurements from radiosondes, for instance. The model’s spectral resolution for this area varies from T450 to T230 (the corresponding smallest resolvable wavelength varies

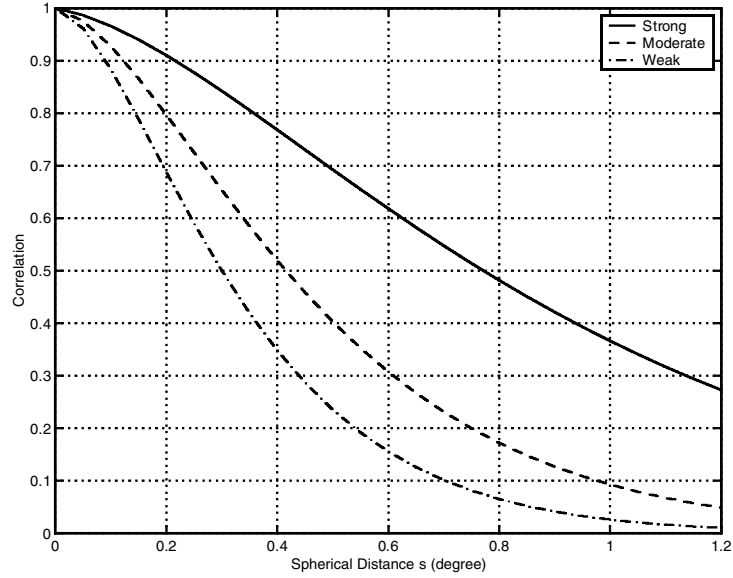


Figure 3. Correlation models of observational noise (see text).

from 89 km to 174 km). In the selected area, there are 3066 Gaussian grid points. The interval of adjacent Gaussian grid points varies from 28 km to 78 km. Note that the average Gaussian grid interval for the incremental analysis with a T95 truncation is about 140 km, which is coarser than the interval of the simulated observations.

Two kinds of observational-noise model were considered: uncorrelated and horizontally correlated. No vertical correlation was considered. The horizontal correlation model is compactly supported and given by

$$\rho(s) = \begin{cases} \left(1 - \frac{s}{s_0}\right) e^{-s/s_0} \left(1 - \frac{s}{s_1}\right), & s \leq s_1, \\ 0, & s > s_1, \end{cases} \quad (1)$$

where s stands for the spherical separation in degrees between two data points. s_0 and s_1 are, respectively, the correlation scale and the cut-off distance beyond which the correlation becomes zero. We chose parameters in Eq. (1) so that the correlation between two grid-points separated by 0.6° reach 0.6, 0.3, 0.15 for strong, moderate and weak correlation models, respectively. The cut-off length s_1 was set to 5° . The correlation models are shown in Fig. 3. One sees that, even for the weak correlation model, the correlation for a 0.3° interval can reach 0.5. The standard deviation of the temperature error was taken as 1.5 K for all 31 model levels. The surface-pressure error corresponds to an amplitude of 8 m in geopotential height. These values were taken from the standard deviations of the radiosonde observation errors and are comparable to the background-error standard deviation specified in the model. In general, the correlated error is more structured than the uncorrelated error. One can note the fact that, with a large correlation, the noise has more chance to be of the same sign in an area. That is, the correlated error has a similar feature to a bias in a local or short time range.

TABLE 1. ASSIMILATION EXPERIMENTS

Experiment	Correlation	Interval ($^{\circ}$)
NOE0.3	No error	0.3
NOC0.3	No correlation	0.3
NOC0.6	No correlation	0.6
NOC1.0	No correlation	1.0
WEA0.3	Weak correlation	0.3
WEA0.5	Weak correlation	0.5
WEA0.6	Weak correlation	0.6
WEA1.0	Weak correlation	1.0
MOD0.3	Moderate correlation	0.3
MOD0.6	Moderate correlation	0.6
MOD0.7	Moderate correlation	0.7
MOD1.0	Moderate correlation	1.0
STR0.3	Strong correlation	0.3
STR0.6	Strong correlation	0.6
STR1.0	Strong correlation	1.0

(c) *Basic assimilation experiments*

Table 1 gives the basic assimilation experiments according to the observation-error correlation and the thinning interval. The assimilation procedure used only some subsets of the total 3066×32 observations (31 levels for temperature T , one level for surface pressure P_s) with different thinning intervals. In the operational system, the thinning of various observations is performed in a rather ad hoc way. The interval between observations usually corresponds to a distance chosen to be in between the analysis mesh and the length-scale of the background-error correlations. In this study, three main intervals corresponding to 0.3° , 0.6° and 1.0° ($1^{\circ} = 111.2$ km along a great circle) were chosen to test the impact of different observation densities. The corresponding number of thinned observations in the horizontal were 2951, 1092 and 401, respectively. Two additional experiments with thinning intervals of 0.5° and 0.7° were performed for the weakly and moderately correlated cases (WEA0.5 and MOD0.7), respectively, for which the adjacent observations have the same correlation value of 0.22. In addition, after some tests, we removed the temperature observations below 970 hPa which could yield spurious analysis increments on the surface pressure. The first experiment NOE0.3 used perfect observations (although a standard deviation of error equal to 1.5 K was still specified in the observation-error covariance) and the highest density of observations. This experiment should have a better analysis quality than the experiments with noisy observations and can be considered as the reference experiment.

(d) *Results with perfect observations*

As shown by Doerenbecher and Bergot (2001), the impact of observations on the forecast is governed by the combination of the sensitivity of the forecast to the initial conditions and to the actual initial errors. The observations that give the maximum impact are not necessarily located in the area with the largest sensitivities. It is, therefore, necessary first to verify if the observations located in the area selected according to the sensitivity field will produce a significant impact in our case. To investigate this, an assimilation experiment named NOE0.3 with perfect observations was performed. Figure 4 shows the 48-hour surface-pressure forecast from this experiment. One can see that the value of the central pressure (969.9 hPa) is very close to that of the ‘truth’ (968.17 hPa), and the position of the centre is perfectly predicted. The forecast of the geopotential height (not shown) is also very close to the truth. The chosen sensitive area is thus considered to be satisfactory and is used in the following experiments.

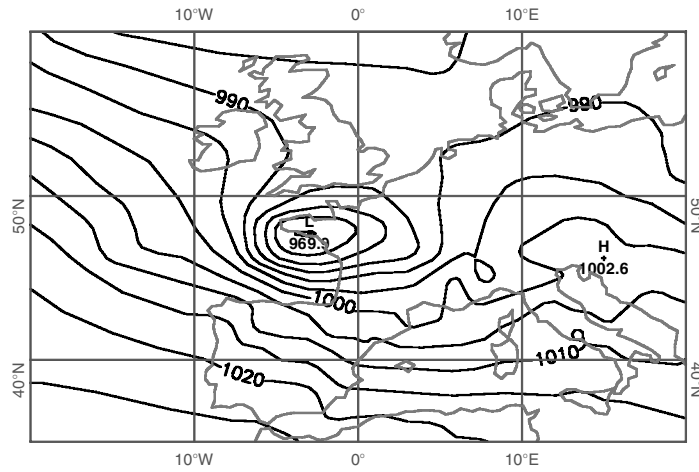


Figure 4. The 48-hour mean-sea-level pressure (hPa) forecast for experiment NOE0.3 with perfect observations (contour interval 5 hPa). See text for further details.

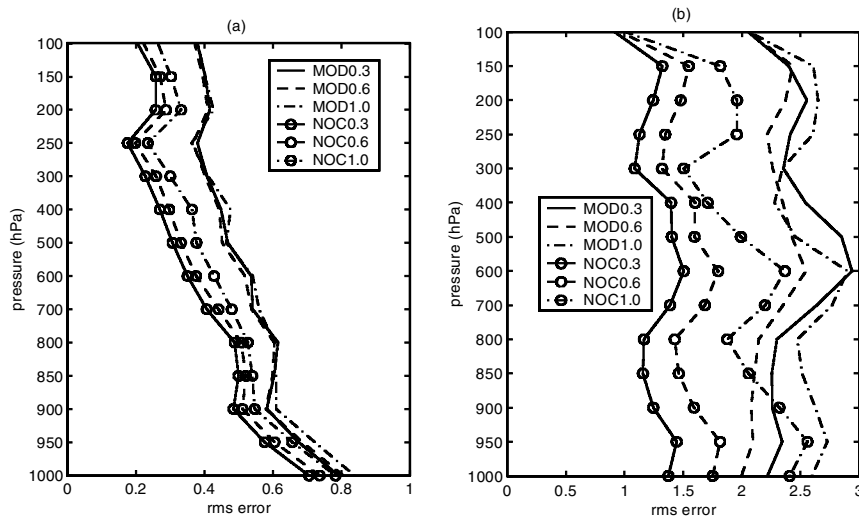


Figure 5. The root-mean-square temperature error (K) of (a) the analysis and (b) the 48-hour forecast for six experiments assuming uncorrelated errors (circles) or moderately correlated errors (no circles). The results are the average of ten random realizations.

(e) Impact of error-correlation strength

The observations with uncorrelated and correlated errors described in section 3(b) were assimilated into the system and then a 48-hour forecast was performed for each assimilation experiment. In order to obtain results that are more significant from a statistical point of view, each experiment was repeated ten times using different error realizations. The results shown are the average over ten random realizations.

Figure 5 shows the root-mean-square (r.m.s.) errors of the analysis and the 48-hour forecast for the temperature at the standard pressure levels. The figure shows the results for only six experiments with uncorrelated and moderately correlated observation

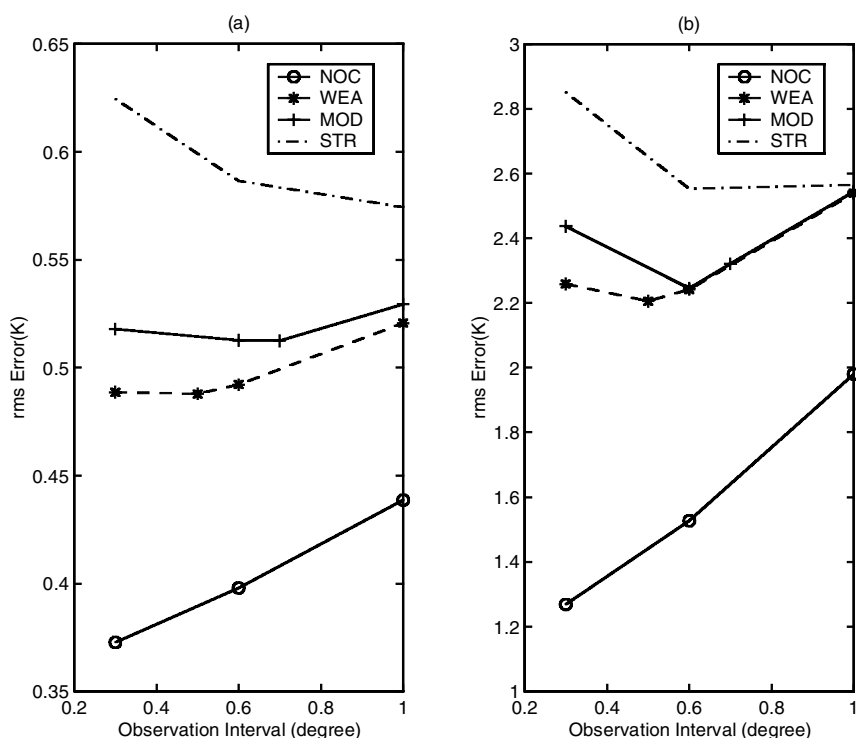


Figure 6. The root-mean-square temperature error averaged over all model levels in (a) the analysis and (b) the 48-hour forecast for experiments with weakly correlated (WEA), moderately correlated (MOD), strongly correlated (STR), and uncorrelated (NOC) observation errors.

errors and with thinning intervals 0.3° , 0.6° and 1.0° . The r.m.s. errors of the analysis were computed over the sensitive area where the simulated observations were located. The r.m.s. errors of the forecast were computed over the targeted area where the storm hit. One notes that the results for uncorrelated and correlated errors exhibit different characteristics. For the former, the r.m.s. errors (for both the analysis and the forecast) clearly reduce with increases in the number of observations, at all levels in the vertical. For correlated errors, we note that the r.m.s. errors (for both the analysis and the forecast) do not decrease or increase monotonically with the observation interval. At most levels in the analysis, a minimum error appears for the observation interval equal to 0.6° . This result is consistent with those obtained in a one-dimensional study (LR2002, Fig. 9), where a minimum error was also found at a given observation interval that was intermediate between fine and coarse for the sub-optimal scheme (i.e. with no modelling of the observation-error correlation in the analysis scheme). For the correlated cases, the variation of forecast errors with observation interval is not completely the same as that of analysis errors. The distinction between the forecast error curves is enhanced, showing the clear advantage of the 0.6° observation interval. Comparing the uncorrelated and correlated cases, one can see that the r.m.s. errors of the analysis and the forecast for the uncorrelated cases are generally smaller than for the correlated cases, as expected. The variation of analysis errors with observation number is smaller for the correlated cases.

Figure 6 shows the r.m.s. temperature errors, averaged over all model levels. The results for the mean-sea-level (MSL) pressure are very similar to those in Fig. 6 and are not shown. One can see that the analysis and forecast errors regularly increase with an increase of the error correlation. More interestingly, the variation of error with the observation interval exhibits a gradual transition from the uncorrelated case to the strongly correlated case. For instance, the error decreases monotonically with the observation interval for the uncorrelated case and increases monotonically for the strongly correlated case. A minimum error is located at an intermediate interval for the weakly correlated and moderately correlated cases. This intermediate interval with a minimum error for the analysis is 0.5° for the weakly correlated case and 0.7° for the moderately correlated case. For these two optimal intervals, the adjacent observations have the same correlation (0.22) which is close to the value 0.15 found by LR2002. Combining with the results found for the forecast error, it would be reasonable to suggest that a threshold correlation of about 0.15–0.3 between adjacent observations should be used to determine the optimal thinning interval. It is important to note that the 48-hour forecast errors may be four to five times larger than the initial analysis errors for the level-averaged temperature (Fig. 6) and ten times larger for the MSL pressure (not shown). The difference of the forecast error between different observation intervals can be an order of magnitude larger than that of the analysis error. For example, the reduction of 0.04 K of the temperature analysis error for the experiment NOC0.6 relative to the experiment NOC1.0 leads to a reduction of 0.45 K of the forecast error (Fig. 6, solid lines with circles).

Figure 7 shows the MSL pressure forecast for the same six experiments as in Fig. 5. One can see that the three worst forecasts are from experiments MOD1.0 (Fig. 7(f)), NOC1.0 (Fig. 7(c)) and MOD0.3 (Fig. 7(d)). Their central pressures are 974.6 hPa, 974.4 hPa and 973.4 hPa, respectively. The results for the other three experiments are not visually very different and the difference in central pressure between them is less than 1 hPa. These are in agreement with the corresponding r.m.s. errors.

(f) *Posterior diagnostic of the sub-optimality of the assimilation scheme*

In the context of statistical linear estimation, Bennett *et al.* (1993) and Talagrand (1998) showed that the cost function at the minimum obtained after minimization is given by

$$J_{\min} = \mathbf{d}^T [\mathbf{H}\mathbf{B}\mathbf{H}^T + \mathbf{R}]^{-1} \mathbf{d}, \quad (2)$$

where \mathbf{H} is the observation operator, \mathbf{B} and \mathbf{R} are, respectively, the background and observation-error covariances specified in the cost function, and $\mathbf{d} = \mathbf{y} - \mathbf{H}\mathbf{x}_b$ is the difference between the observation \mathbf{y} and the background \mathbf{x}_b (usually called the *innovation vector*). The superscripts T and -1 represent, respectively, the transpose and inverse operators. Note that a factor $\frac{1}{2}$ has been removed in the definition of the cost function. The statistical average of J_{\min} can be shown to be equal to the observation number N if the analysis scheme is optimal (i.e. if the error covariances \mathbf{B} and \mathbf{R} are correctly specified). This fact can be used as an a-posteriori diagnostic of the statistical optimality of the assimilation system. The assimilation scheme used in our OSSEs was sub-optimal for the case with correlated observation error because of the use of a diagonal covariance matrix \mathbf{R} . This sub-optimality should be revealed in the statistics of J_{\min} . Figure 8 shows J_{\min}/N as a function of observation interval for the uncorrelated, weakly-correlated, moderately correlated and strongly correlated cases. We note that, for the uncorrelated case for which the assimilation scheme is thought to be optimal, J_{\min}/N is slightly larger than 1, which might be a consequence of underestimating the background-error

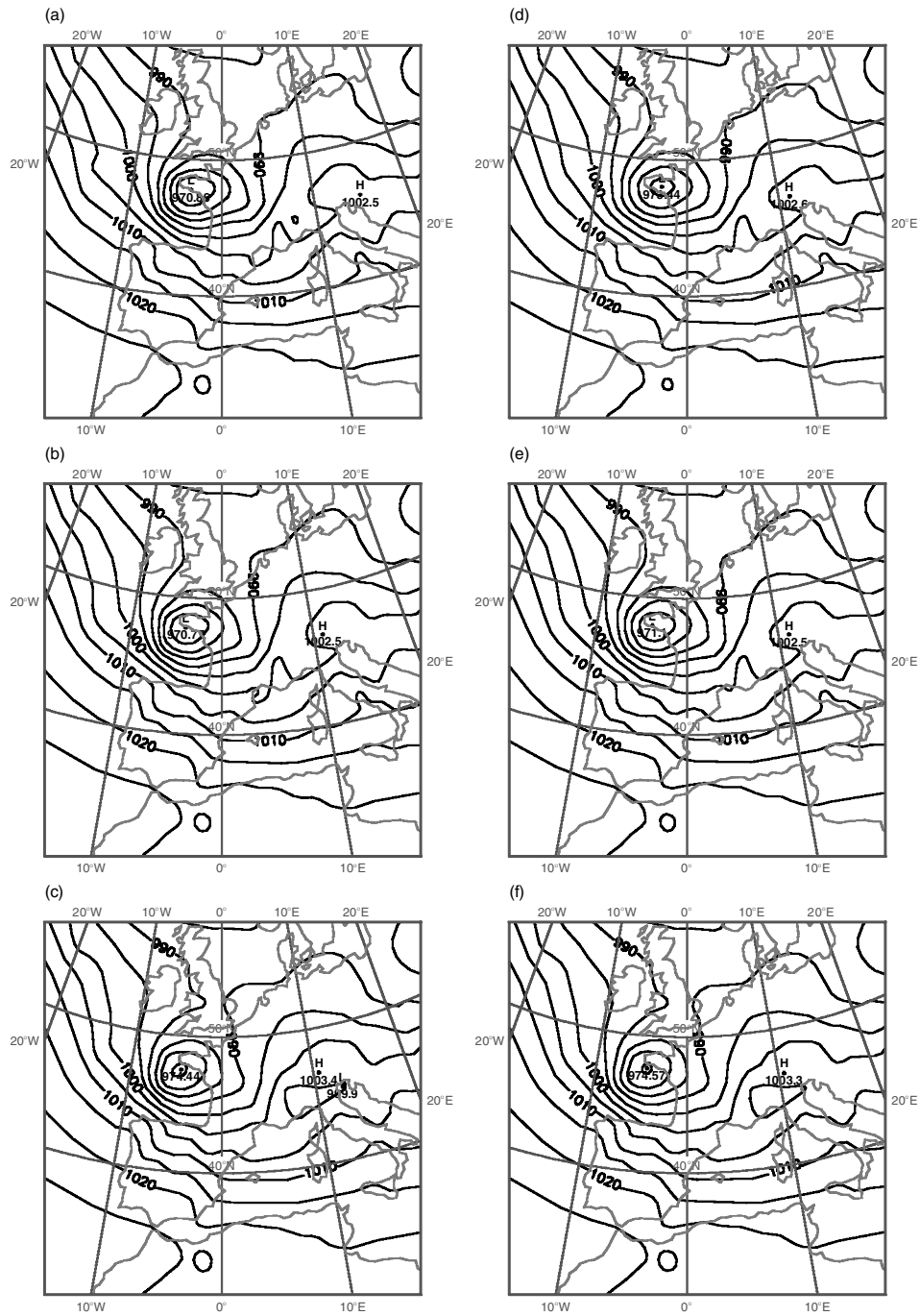


Figure 7. The mean-sea-level pressure (hPa) of the 48-hour forecast for six experiments: (a) NOC0.3; (b) NOC0.6; (c) NOC1.0; (d) MOD0.3; (e) MOD0.6; and (f) MOD1.0.

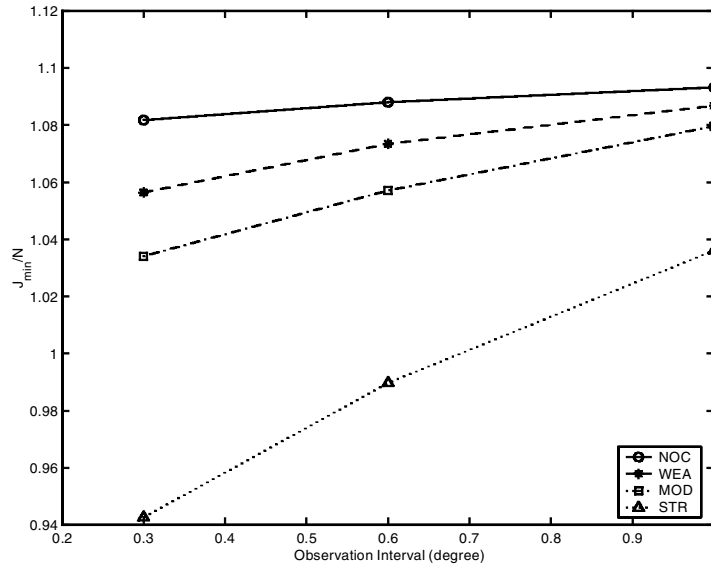


Figure 8. The cost function at minimization, J_{\min} , normalized by the observation number N , as a function of observation interval for experiments with weakly correlated (WEA), moderately correlated (MOD), strongly correlated (STR), and uncorrelated (NOC) observation errors.

variance in the covariance matrix \mathbf{B} . An important remark is that J_{\min}/N decreases with the increase of the observation-error correlation. This is also revealed by the fact that J_{\min} decreases with the decrease of observation interval, which also leads to the increase of error correlation.

It should be mentioned that completely uncorrelated errors (so-called white noise), which imply that the error power is distributed uniformly over all spectral components in the full infinite range, are not physically realizable (Gelb *et al.* 1974, p. 42). A tiny correlation could exist for the uncorrelated-error case. This is the reason why a slight decrease of J_{\min} with the observation interval can also be observed for the uncorrelated case. The results for J_{\min}^o (the observation part of the cost function at the minimum) is similar to those in Fig. 8 (not shown). It is known that, for the correlated case, the drawback of the sub-optimal scheme can be partly compensated by increasing the observation error σ_o in the matrix \mathbf{R} . This has been verified by performing additional experiments for the strongly correlated case with a 10% increase in σ_o . The analysis error is reduced by about the same amplitude (Fig. 9). From Eq. (2), an unavoidable consequence of increasing σ_o is the further reduction of J_{\min} (also J_{\min}^o). In our case, a reduction of about 0.2 in J_{\min} is observed for all three thinning intervals. This feature suggests that one should be careful to use an algorithm for tuning the observation-error parameters that is based on the diagnostics of J_{\min} or J_{\min}^o (Desroziers and Ivanov 2001) for observations with correlated errors and when using a sub-optimal scheme. In this case, the algorithm will tend to reduce σ_o to 1 when approaching the value of J_{\min} , and so lead to an increase of the analysis error. It is also noted that the variation of J_{\min}/N with the correlation strength is not very large, e.g. from 1.08 for the uncorrelated case to 0.94 for the strongly correlated case with an interval of 0.3° (corresponding to a correlation of 0.85). This means that it is difficult to use J_{\min} to diagnose the sub-optimality of the assimilation system resulting from deficiencies in modelling the observation-error correlation.

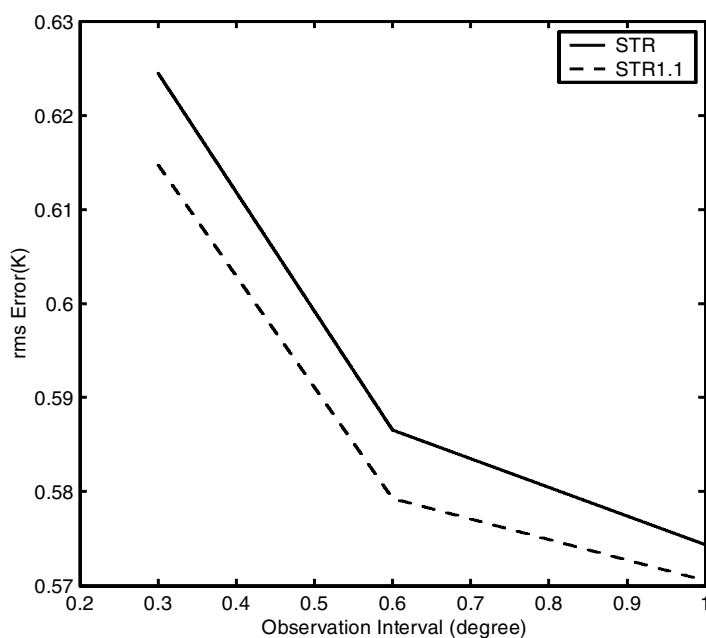


Figure 9. The root-mean-square error of the temperature analysis (K) averaged over all vertical levels for strongly correlated observation-error experiments with the specified value of the observation error σ_o equal to the correct value 1.5 (solid line) and 1.5×1.1 (dashed line). See text for further information.

4. CONSISTENCY OF HORIZONTAL AND VERTICAL RESOLUTIONS

Note that, in the above experiments, since the simulated observations are located on all model levels, the vertical resolution of the measurements can be regarded as perfect. One might ask the following question: are horizontally dense observations still preferred if there is poor vertical resolution, even when the observation errors are uncorrelated? This was examined by assimilating observations with fewer vertical levels, namely those that correspond to the heights of some AMSU-A channels. Only the experiments with uncorrelated observation errors were performed. In the following, subsection 4(a) presents the experimental results using fewer levels of temperature in the same context as in section 3, and subsection 4(b) gives the results for simulated AMSU-A radiances in another meteorological situation expected to have good data coverage by two NOAA satellites (NOAA15 and NOAA16).

(a) Experiments with fewer temperature levels

It was noted by Lindzen and Fox-Rabinovitz (1989) and Fox-Rabinovitz and Lindzen (1993) that a consistent relation exists between vertical and horizontal resolution for the discretization of NWP models. Fine horizontal resolution accompanied by a poor vertical resolution can produce increased analysis noise. They also suggested that these consistent relations could be applied to observing systems. To investigate this issue in our context, vertical thinning was performed to artificially reduce the resolution of the observations in the vertical. The surface-pressure observations were the same as in the previous experiments, and the temperature observations were used at only seven model levels (600, 400, 200, 150, 100, 50 and 30 hPa) corresponding to the pressure levels of peak values of the weighting functions for AMSU-A channels 5 to 11, which

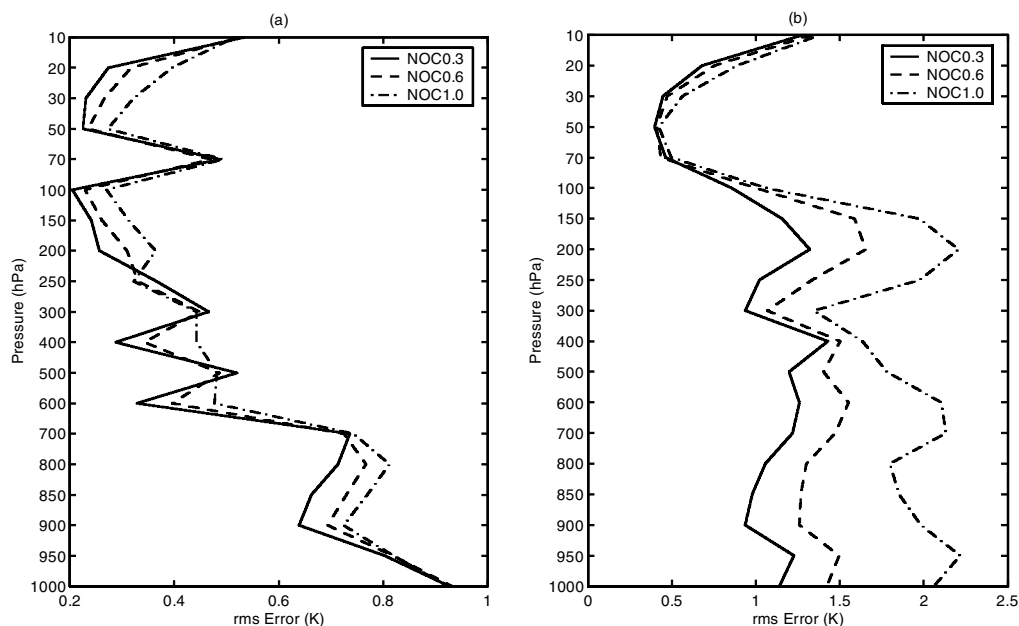


Figure 10. The root-mean-square temperature error (K) of (a) the analysis and (b) the 48-hour forecast for three experiments with uncorrelated errors and fewer vertical observing levels (see text).

are currently used in the assimilation system at Météo-France. The horizontal observation intervals were also comparable with those of AMSU-A raw radiances (they vary from 50 km at nadir to 110 km at the limb). Figure 10 shows the r.m.s. temperature errors for the uncorrelated cases. The horizontal thinning was the same as discussed in the previous section. One can see that the maximum analysis error reductions are at the levels where the observations are located. It should be mentioned that the analysis error could not show such distinct peaks for radiance measurements because of broad channel-weighting functions. Moreover, the benefit obtained at these levels at the initial time is propagated in the vertical and leads to an improvement of the forecast at most levels. Also note that, at some levels without observations (e.g. 500 hPa), the analysis error increases for a small thinning interval, although by a small amount in this particular experiment. This is further illustrated and explained in the next subsection for OSSEs with radiances.

(b) *Experiments with simulated AMSU-A radiances*

(i) *Meteorological situation and simulated observations.* At 00 UTC 21 September 2001, the 96-hour forecast of the ARPEGE model has a large error over North America (Fig. 11(b)). ARPEGE displaced the troughs so quickly that the predicted ridge/trough system was in the opposite phase compared with the analysed ridge/trough system, whereas the European Centre for Medium-Range Weather Forecasts (ECMWF) model gave an almost perfect prediction (not shown). Figure 11(a) shows the forecast by ARPEGE starting from the ECMWF analysis. This forecast is very close to the valid ARPEGE analysis (not shown) and was considered as the truth (at forecast time) in the OSSEs. The maximum error in the geopotential height at 500 hPa reaches ± 300 m (Fig. 11(c)). At that time, both Météo-France and ECMWF operated a 4DVAR

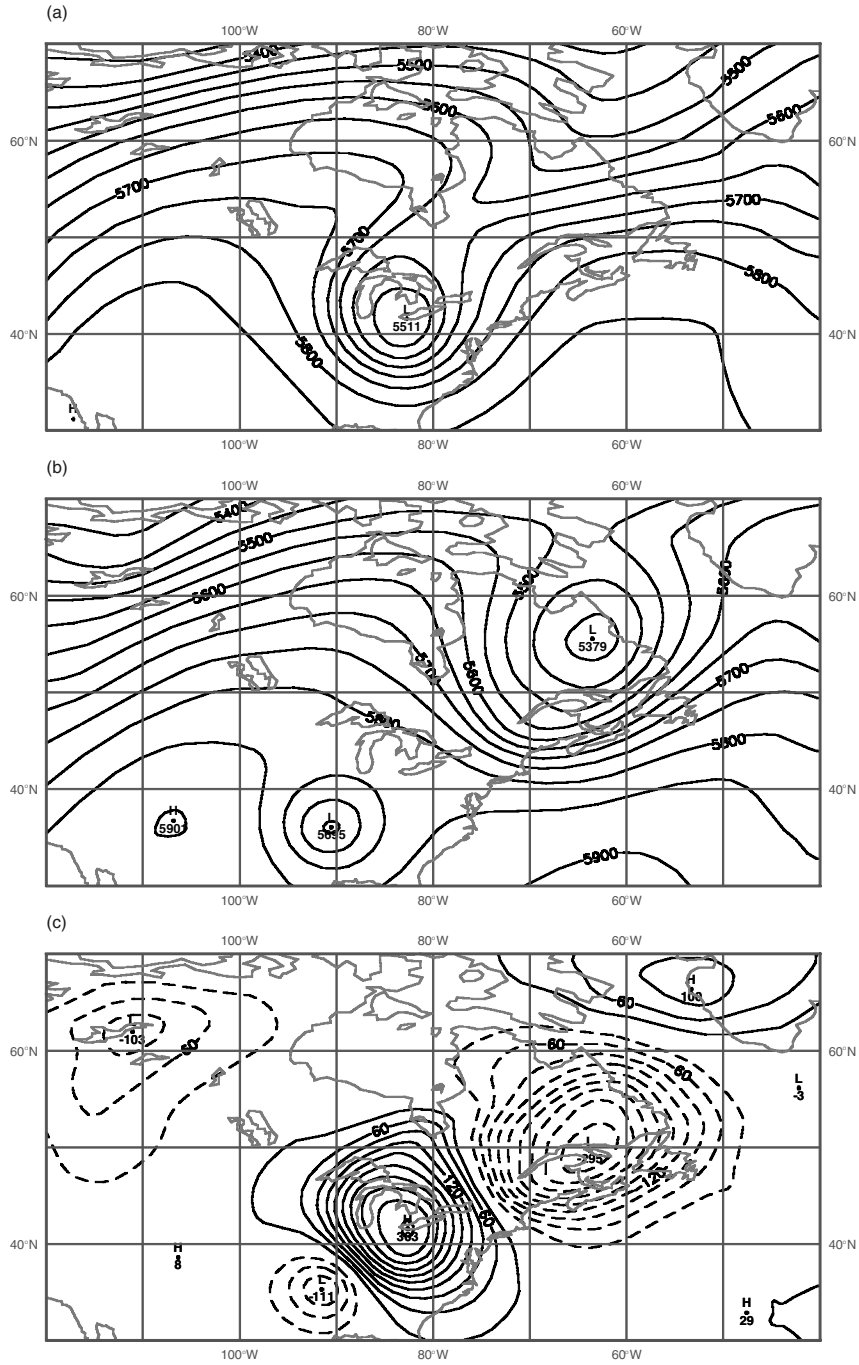


Figure 11. The 96-hour forecast of the 500 hPa geopotential height (m) valid at 00 UTC 25 September 2001 starting from (a) the ECMWF initial conditions, and (b) the ARPEGE initial conditions. (c) The difference (b) minus (a).

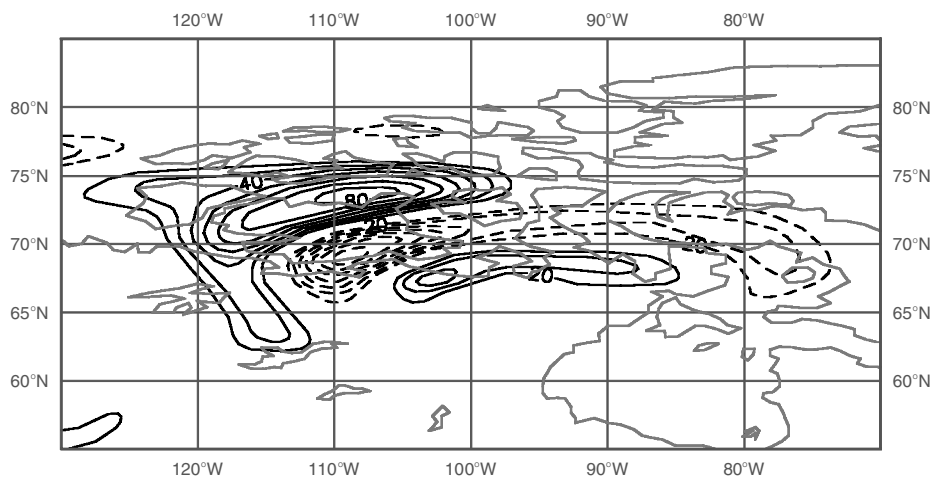


Figure 12. The gradient field, with respect to the 500 hPa temperature at 00 UTC 21 September 2001, of the cost function that was the norm of the 96-hour forecast error valid at 00 UTC 25 September 2001. The contour interval is 10 K and the gradient value shown has been divided by 100.

assimilation system. However, one of the major differences between the two systems was that ARPEGE used a different set of observations than the operational system at ECMWF. In particular, ECMWF assimilated raw radiances (McNally *et al.* 2000) instead of the NESDIS pre-processed 120 km ‘cloud-cleared’ radiances that were used in ARPEGE at that time (at 250 km resolution). This case is then possibly thought to be a good one for testing the impact of assimilating raw radiances. At the time of this study, only experimental runs of assimilating raw radiances had been performed with ARPEGE.

An examination of the differences between the trajectories forecast by the ECMWF and ARPEGE systems indicates that the large errors in the 96-hour forecast were mainly due to initial errors in the north of North America. We also performed sensitivity computations by means of an adjoint integration for $T + 96$ hours (though the condition of linear evolution of errors was not strictly checked). Figure 12 shows the gradient field for temperature at 500 hPa, the level where the gradient field exhibits the largest values. The coverage area is consistent with that determined by examination of the trajectory of forecast differences. This, therefore, helps us to determine our ‘sensitive area’. Observations were inserted in a broader area, which we defined as the area north of 50°N over North America, which includes this sensitive area.

The simulated observations were AMSU-A radiances with real orbit positions in a six-hour assimilation window centred at 00 UTC 21 September 2001. Only channels 5 to 12 were used. Recalling section 3, the simulated radiances were obtained by adding a random error (uncorrelated) to the ‘true’ radiances computed from the ECMWF analysis field. In the context of OSSEs, observation operators, such as the radiative-transfer model (RTM), were considered as perfect. Consequently some common quality controls (such as cloud and land–sea checks for real radiance data) were not necessary, and only observations having large departures from the background were rejected. This ensured that we kept enough observations to test the impact of different observational thinning. No other observations were used in the assimilation. The background field for the assimilation experiments was the same as the ARPEGE operational one.

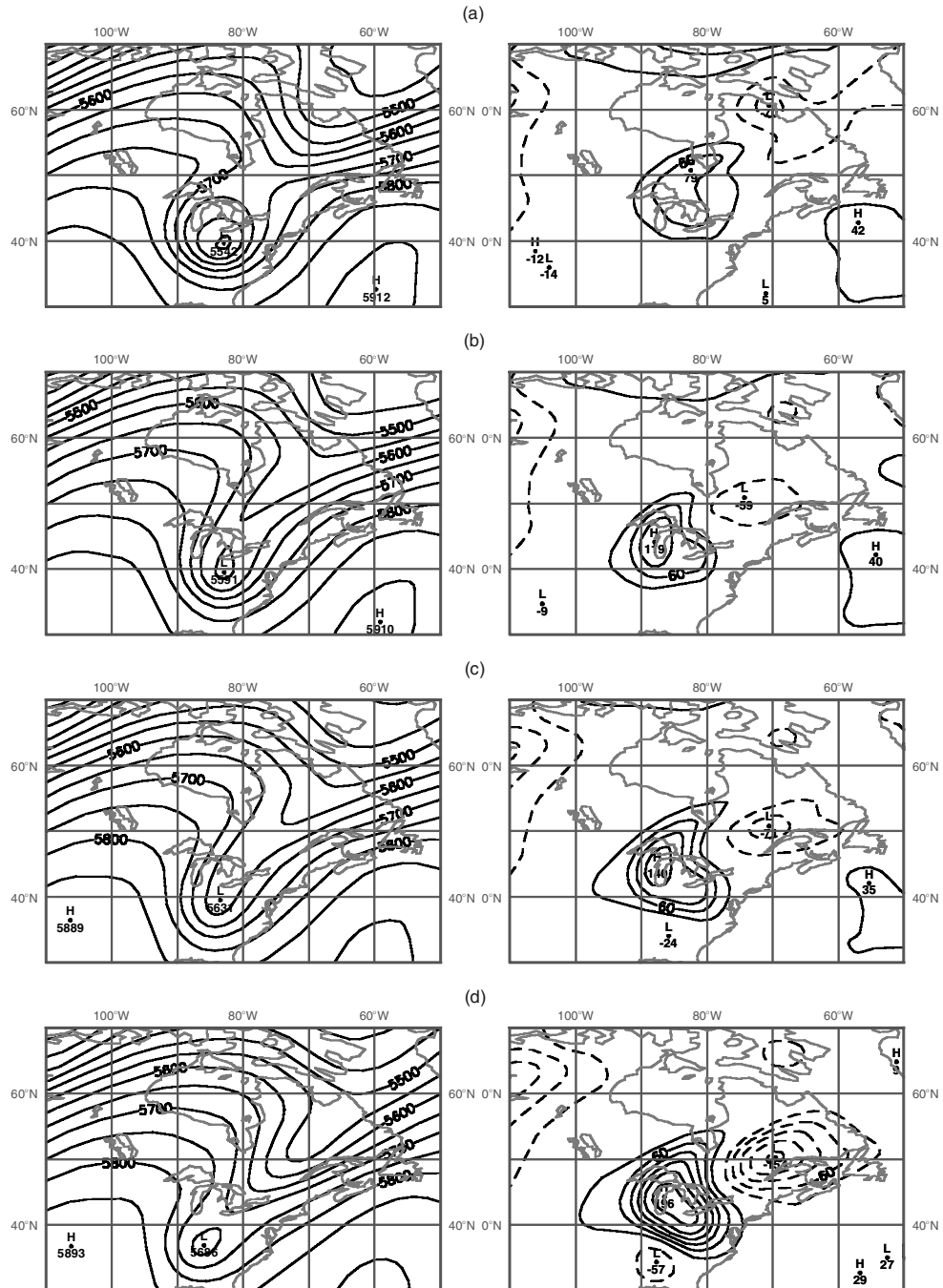


Figure 13. The 96-hour forecasts (left-hand panels) and the forecast errors with respect to the ECMWF forecasts (right-hand panels) of the 500 hPa geopotential height (m) valid at 00 UTC 25 September 2001 for experiments (a) perfect observations without thinning (corresponding to a minimal interval of 50 km at nadir), (b) noisy observations without thinning, (c) noisy observations with a thinning of 1°, and (d) noisy observations with a thinning of 2°. For the experiments with noisy observations, the results are the average of ten realizations.

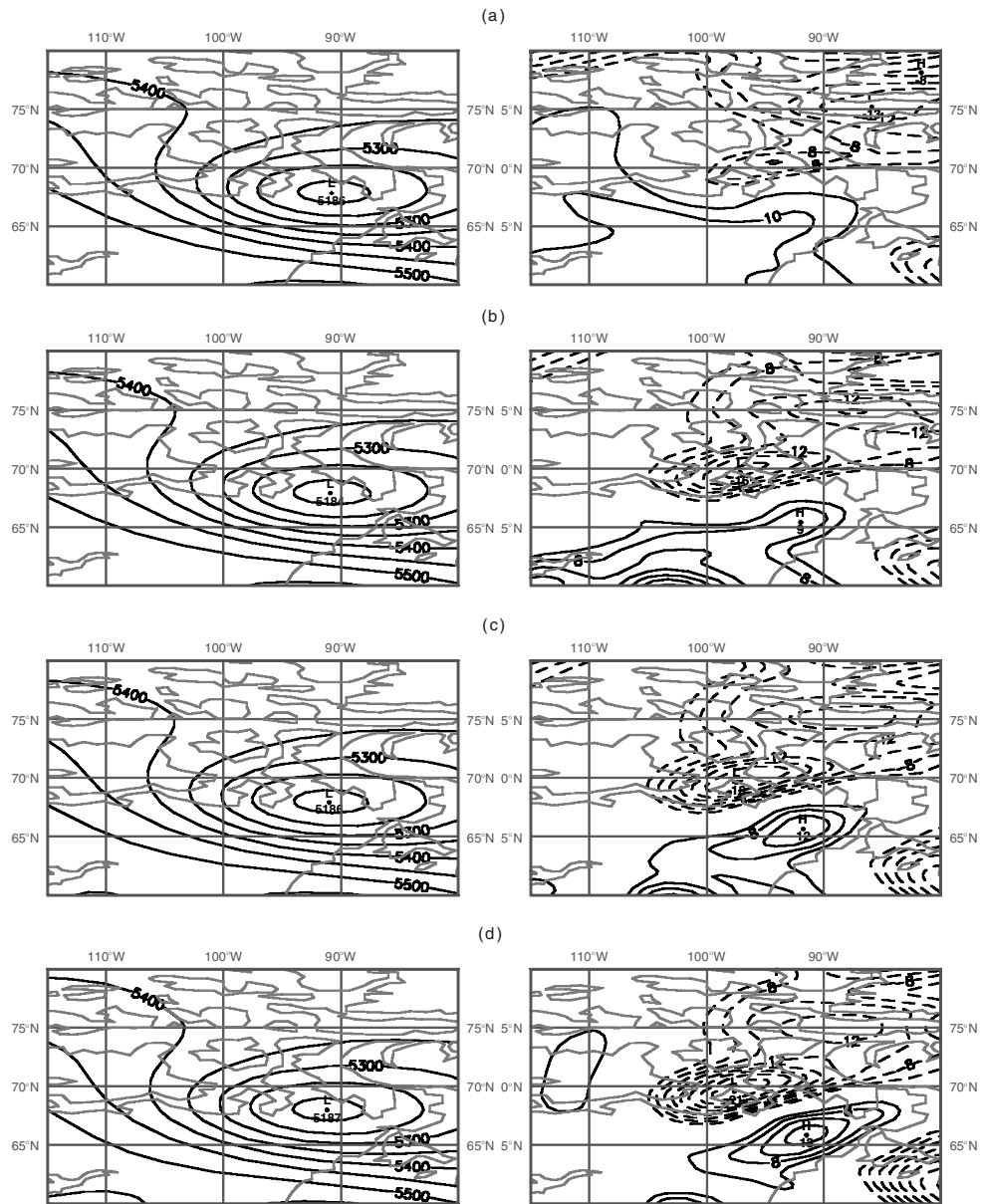


Figure 14. As Fig. 13, but for the corresponding analyses at 00 UTC 21 September 2001 (left-hand panels) and the analysis-error fields (right-hand panels) in the sensitive area.

(ii) *Experiment results.* Figure 13 indicates that the improvement of the forecasts (compared with Fig. 11(b)) is considerable. For the two cases without thinning, the maximum forecast error is reduced from about 300 m to 79 m for perfect observations and 119 m for noisy observations. The forecast is degraded with a decrease in observation number. The corresponding analysis fields and analysis-error fields in the sensitivity area are shown in Fig. 14. The variation of the analysis error with observation interval is consistent with that of the 96-hour forecast error. This suggests that retaining

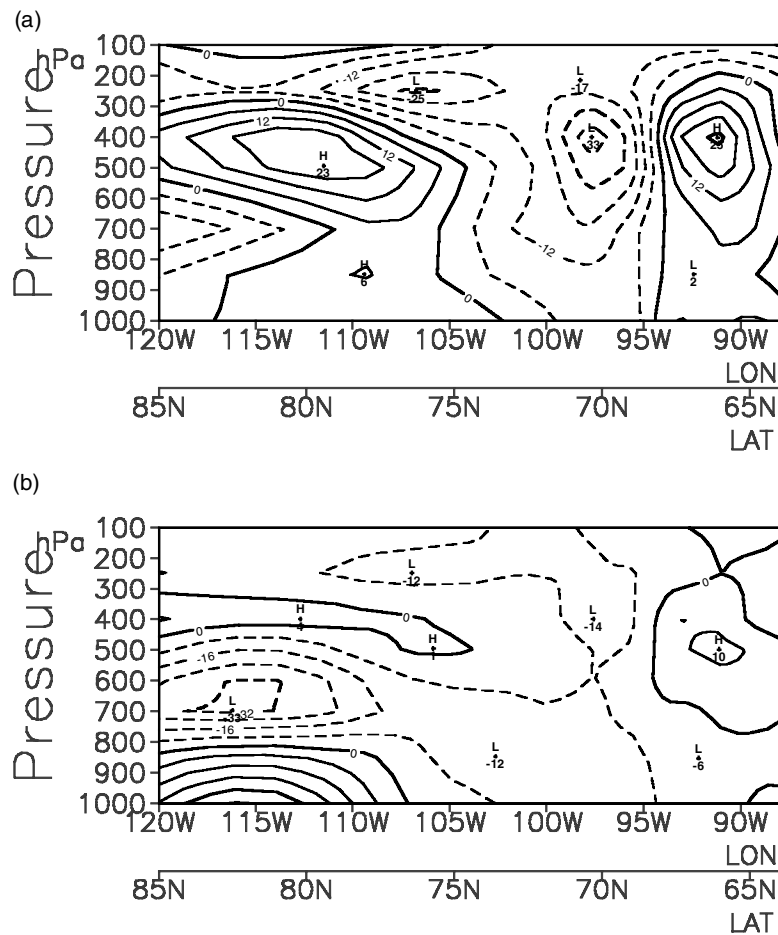


Figure 15. Cross-sections along the line from (85°N, 120°W) to (64°N, 88°W) (m) of (a) the background errors of the geopotential height, and (b) the analysis errors with perfect observations (m).

a large number of observations is essential for a reduction of the main error in some sensitive areas. Note the fact that only simulated radiances, which are associated with the temperature and humidity profiles as well as with the surface pressure by the RTM in a complex way, are assimilated in the experiments. This demonstrates the capability of indirect measurements, such as radiances, to recover the atmospheric state and thus improve the subsequent forecast, consistent with operational experiments (English *et al.* 2000; Bouttier and Kelly 2001).

However, we also note from the computation of the r.m.s. analysis error that, unlike the result in section 4(a), the analysis error is not systematically reduced with an increase in the observation number in the entire region of observation coverage and at all vertical levels. The reasons might be complex, and possibly linked to the specification of the structure functions used in the analysis. The inconsistency of the vertical analysis error can be illustrated by a cross-section of the geopotential-height error along a line crossing the sensitive area from (85°N, 120°W) to (64°N, 88°W) at the initial time, as shown in Fig. 15. One can see that the background error is significantly reduced above

500 hPa by the assimilation of radiance observations, but below 500 hPa the analysis error is much larger than the background error from 120°W to 110°W. One recalls that the height of the peak value of the weighting function for channel 5 (the lowest channel) is about 600 hPa. The corrections of the background field at low levels are expected to come mainly from the propagation of analysis increments by the structure functions at high levels. Clearly, the negative background errors in the lower-left part of the figure is further increased by negative analysis increments that are produced by observations between 300 hPa and 600 hPa. From this point of view, it is necessary to retain a certain balance of observations between the horizontal and vertical directions to reduce the influence of incorrect propagation of analysis increments. However, this does not mean that there is an internal consistency-relation between the horizontal and vertical resolutions of the observations. We think that the problem is essentially due to the weakness of the structure functions used in the analysis. In general, the 4DVAR assimilation can benefit from the implicit dynamical structure functions (Thépaut *et al.* 1996). However, most operational centres currently use a constant background-error covariance matrix obtained from the statistics of the differences between different ranges of forecasts (Parrish and Derber 1992), which constrains the advantage of the 4DVAR assimilation, particularly when using a six-hour assimilation window (Rabier *et al.* 2000). A perfect structure function, by definition, should statistically be able to propagate information correctly from one place to another or from one variable to another. This can only be achieved by introducing flow-dependent background-error covariances and cycling them from one analysis to the next one.

5. CONCLUSIONS

In this paper, the potential of high-density observations on NWP has been studied by examining two ‘difficult’ meteorological situations for which the operational ARPEGE model failed to produce the correct forecasts. Simulated observations with different error features and different thinning intervals were used in the study. The results confirm some remarks found by LR2002 in a simple 1D context: for observations with uncorrelated errors, increasing the observation density generally improves the analysis and the forecast; even for observations with correlated errors and using a sub-optimal scheme (i.e. no modelling of this error correlation), the assimilation system can still extract some useful information, and a minimum error for the analysis and forecast is also found for some intermediate observation interval; the threshold value of the error correlation for optimal thinning interval is around 0.2. Each OSSE was performed ten times with different random-error realizations. The results are then expected to be meaningful in a statistical sense, although the study was directed at only two particular meteorological situations. Recently, Bormann *et al.* (2003) have shown that atmospheric motion vectors derived from geostationary satellite imagery exhibit statistically-significant spatial error correlations. However, one should be careful in applying the threshold correlation value to guide the determination of an optimal thinning interval for atmospheric motion vectors since the results in this paper have been obtained from experiments using simulated temperatures. We should also recognize the limitation of the identical-twin type OSSE methodology used in this study. In the identical-twin experiment context only forecast errors due to initial conditions are represented, and the assimilation system can extract more information about the ‘truth’ than about the real atmosphere with the same amount of simulated and real observations. It is thus expected that, in this OSSE, data saturation will tend to occur at lower data densities than in practice. This could lead to an underestimation of the impact of observations with extensive data coverage.

Moreover, it is shown that a small improvement in the analysis field in a sensitive area can considerably improve the subsequent forecast, and retaining a high density of observations (the corresponding observation interval may be much smaller than the analysis grid and the background-error correlation-scale) is essential for reducing the key initial error. It is also shown that the sub-optimality of the assimilation scheme for correlated observation errors leads to a decrease in the cost function normalized by the observation number at minimization, J_{\min}/N , as the observation-error correlation strength increases. This suggests that tuning the observation-error parameters (e.g. the error standard deviation) according to J_{\min}/N is problematic for correlated observations, and should be applied with caution and in conjugation with other criteria.

A risk of using high-density observations is that it might produce false large increments and degrade the analysis in some levels with no observations, although this degradation might not necessarily influence the forecast in the interesting area, as shown for the second case. We think that this problem comes mainly from the weakness of the background-error covariance which, in current operational practice, is often taken as a constant matrix and can, in some situations, propagate information incorrectly from one place to another, or from one variable to another. The introduction of a flow-dependent background-error covariance in the future is expected to be able to overcome this kind of problem. From the point of view of improving forecasts in regions of interest, a high observation density in sensitive areas is preferred (e.g. upstream) even if it only extends to a limited number of vertical levels. Gelaro *et al.* (2000) have shown in an experiment during a three-week period that high-density geostationary-satellite wind data provided substantial improvements in 48-hour forecast skill, and that the improvements resulted mainly from the reduction of the key analysis error in the middle and lower troposphere where more satellite wind data are located.

LR2002 and Bergman and Bonner (1976) also showed that, for correlated observations, increasing the observation density beyond a threshold value yields little or no improvement in analysis accuracy, even when the error correlation is correctly modelled in the observation-error covariance. It would be interesting to test further the impact of modelling the observation-error correlation in a practical 4DVAR assimilation context. Lorenc (1992) suggested approximating the inverse of the error covariance matrix using filters, which is a potential method of treating the correlated observation errors. The statistics of observation errors (in particular their correlation) is important both for the purpose of their modelling and of optimal observation thinning, and it constitutes a challenging task. Finally, it should be mentioned that another possible option for using high-density observations is to assimilate them as 'super-observations' (Lorenc 1981) produced by combining the *innovations* in a neighbouring area. This process has the advantage of being able to increase the representativity of the observation and to reduce, to some degree, the observation error. It is still not clear whether thinning or super-observing observations is better. This should be studied in the future.

ACKNOWLEDGEMENTS

The authors wish to thank Gwenaëlle Hello for the computation of the sensitivity field. Jean Pailleux and Alex Doerenbecher are also gratefully acknowledged for their help in the choice of the second case study. Jean-Noël Thépaut helpfully provided the ECMWF analysis fields. Many people in the GMAP group (particularly Patrick Moll, Dominique Puech, Elisabeth Gérard, Ryad El Khatib, Philippe Caille, Bernard Chapnik and Patrick Saez) are acknowledged for their valuable technical support.

REFERENCES

- Bennett, A. F., Leslie, L. M., Hagelberg, C. R. and Powers, P. E. 1993 Tropical cyclone prediction using a barotropic model initialized by a generalized inverse method. *Mon. Weather Rev.*, **121**, 1714–1729
- Bergman, K. H. and Bonner, W. D. 1976 Analysis error as a function of observation density for satellite temperature soundings with spatially correlated errors. *Mon. Weather Rev.*, **104**, 1308–1316
- Bormann, N., Saarinen, S., Kelly, G. and Thépaut, J.-N. 2003 The spatial structure of observation errors in atmospheric motion vectors from geostationary satellite data. *Mon. Weather Rev.*, **131**, 706–718
- Bouttier, F., and Kelly, G. 2001 Observing system experiments in the ECMWF 4D-Var data assimilation system. *Q. J. R. Meteorol. Soc.*, **127**, 1469–1488
- Charles, P., Arnold, C. P. Jr. and Dey, C. H. 1986 Observing-system simulation experiments: past, present and future. *Bull. Amer. Meteorol. Soc.*, **67**, 687–695
- Courtier, P. and Geleyn, J.-F. 1988 A global numerical weather prediction model with variable resolution: Application to the shallow-water equations. *Q. J. R. Meteorol. Soc.*, **114**, 1321–1346
- Courtier, P., Thépaut, J.-N. and Hollingsworth, A. 1994 A strategy for operational implementation of 4D-Var, using an incremental approach. *Q. J. R. Meteorol. Soc.*, **120**, 1367–1387
- Derber, J. and Bouttier, F. 1999 A reformulation of the background error covariance in the ECMWF global data assimilation system. *Tellus*, **51A**, 195–221
- Desroziers, G. and Ivanov, S. 2001 Diagnosis and adaptative tuning of observation error parameters in a variational assimilation. *Q. J. R. Meteorol. Soc.*, **127**, 1433–1452
- Doerenbecher, A. and Bergot, T. 2001 Sensitivity to observations applied to FASTEX cases. *Nonlinear Proc. Geophys.*, **8**, 1–16
- English, S. J., Renshaw, R. J., Dibben, P. C., Smith, A. J., Rayer, P. J., Poulsen, C., Saunders, F. W. and Eyre, J. R. 2000 A comparison of the impact of TOVS and ATOVS satellite sounding data on the accuracy of numerical weather forecasts. *Q. J. R. Meteorol. Soc.*, **126**, 2911–2931
- Fox-Rabinovitz, M. and Lindzen, R. S. 1993 Numerical experiments on consistent horizontal and vertical resolution for atmospheric models and observing systems. *Mon. Weather Rev.*, **121**, 264–271
- Gauthier, P. and Thépaut, J.-N. 2001 Impact of the digital filter as a weak constraint in the pre-operational 4DVAR assimilation system of Météo-France. *Mon. Weather Rev.*, **129**, 2089–2102
- Gelaro, R., Reynolds, C. A., Langland, R. H. and Rohaly, G. D. 2000 A predictability study using geostationary satellite wind observations during NORPEX. *Mon. Weather Rev.*, **128**, 3789–3807
- Gelb, A., Kasper, J. F., Nash, R. A., Price, C. F. and Sutherland, A. A. 1974 *Applied optimal estimation*. M.I.T. Press, Boston, USA
- Janisková, M., Thépaut, J.-N. and Geleyn, J. F. 1999 Simplified and regular physical parameterization for incremental four-dimensional variational assimilation. *Mon. Weather Rev.*, **127**, 26–44
- Järvinen, H. and Undén, P. 1997 ‘Observation screening and first guess quality control in the ECMWF 3D-VAR data assimilation system’. ECMWF Tech. Memo. 236 (available from the European Centre for Medium-Range Weather Forecasts, Shinfield Park, Reading, Berkshire RG2 9AX, UK)
- Lindzen, R. S. and Fox-Rabinovitz, M. 1989 Consistent vertical and horizontal resolution. *Mon. Weather Rev.*, **117**, 2575–2582
- Liu, Z.-Q. and Rabier, F. 2002 The interaction between model resolution, observation resolution and observation density in data assimilation: A one-dimensional study. *Q. J. R. Meteorol. Soc.*, **128**, 1367–1386
- Lorenc, A. C. 1981 A global three-dimensional multivariate statistical interpolation scheme. *Mon. Weather Rev.*, **109**, 701–721
- 1992 Iterative analysis using covariance functions and filters. *Q. J. R. Meteorol. Soc.*, **118**, 569–591
- Lynch, P., Girard, D. and Ivanovici, V. 1997 Improving the efficiency of a digital filtering scheme for diabatic initialization. *Mon. Weather Rev.*, **125**, 1976–1982
- McNally, A. P., Derber, J. C., Wu, W. and Katz, B. B. 2000 The use of TOVS level-1b radiances in the NCEP SSI analysis system. *Q. J. R. Meteorol. Soc.*, **126** 689–724

- Parrish, D. F. and Derber, J. C. 1992 The National Meteorological Center's spectral statistical-interpolation analysis system. *Mon. Weather Rev.*, **120**, 1747–1763
- Rabier, F., Klinker, E., Courtier, P. and Hollingsworth, A. 1996 Sensitivity of forecast errors to initial conditions. *Q. J. R. Meteorol. Soc.*, **122**, 121–150
- Rabier, F., McNally, A., Andersson, E., Courtier, P., Undén, P., Eyre, J., Hollingsworth, A. and Bouttier, F. 1998 The ECMWF implementation of three-dimensional variational assimilation (3D-Var). II: Structure functions. *Q. J. R. Meteorol. Soc.*, **124**, 1809–1829
- Rabier, F., Järvinen, H., Klinker, E., Mahfouf, J.-F. and Simmons, A. 2000 The ECMWF operational implementation of four-dimensional variational assimilation. I: Experimental results with simplified physics. *Q. J. R. Meteorol. Soc.*, **126**, 1143–1170
- Rabier, F., Fourrié, N., Chafai, D. and Prunet, P. 2002 Channel selection methods for Infrared Atmospheric Sounding Interferometer radiances. *Q. J. R. Meteorol. Soc.*, **128**, 1011–1027
- Talagrand, O. 1998 'A posteriori evaluation and verification of analysis and assimilation algorithms'. In Proceedings of the ECMWF workshop on diagnosis of data assimilation systems, 2–4 November 1998. European Centre for Medium-Range Weather Forecasts, Shinfield Park, Reading, Berkshire RG2 9AX, UK
- Thépaut, J.-N., Courtier, P., Belaud, G. and Lemaitre, G. 1996 Dynamical structure functions in a four-dimensional variational assimilation: A case study. *Q. J. R. Meteorol. Soc.*, **122**, 535–561
- Veersé, F. and Thépaut, J.-N. 1998 Multiple-truncation incremental approach for four-dimensional variational data assimilation. *Q. J. R. Meteorol. Soc.*, **124**, 1889–1908